Making the zeroth-order process fidelity independent of state preparation and measurement errors

Yu-Hao Chen,[1, 2, *] Renata Wong,[2, 3, †] and Hsi-Sheng Goan[1, ‡]

[1] *Department of Physics, National Taiwan University, Taipei, Taiwan*
[2] *Department of Artificial Intelligence, Chang Gung University, Taoyuan, Taiwan*
[3] *Department of Neurology, Chang Gung Memorial Hospital, Keelung, Taiwan*

(Dated: December 22, 2025)

We demonstrate that the zero-fidelity, an approximation to the process fidelity, becomes robust to state preparation and measurement (SPAM) errors when combined with randomized benchmarking. However, as randomized benchmarking requires randomly choosing an increasingly large number of Clifford elements from the Clifford group when the qubit number increases, this combination is also limited to quantum systems with up to three qubits. To make the zero-fidelity independent of SPAM errors and, at the same time, applicable to multi-qubit systems, we employ a channel noise scaling method called zero noise extrapolation and show that this also makes the zero fidelity robust to SPAM errors.

arXiv:2312.08590v3 [quant-ph] 19 Dec 2025

I. INTRODUCTION

As quantum computers are expected to become more powerful for performing calculations than classical computers, quantum computation may one day replace classical computation for some difficult problems. In order to evaluate the performance of real quantum devices, as opposed to classical simulators of quantum processes, one can use the widely used protocol called *process fidelity* [1]. This protocol is known to require a considerable number of experimental settings and frequent changes of initial states and measurement bases on a shot-by-shot case. Recently, another protocol called *zero-fidelity* [2] was proposed, which can be seen as the zeroth-order approximation to the process fidelity and which addresses these issues. However, it has not yet been shown how the zero-fidelity protocol can be quantified to make it independent of state preparation and measurement (SPAM) errors, which limit the usefulness of the zero-fidelity for real devices.

It has been demonstrated in [1, 3] that, in general, one can use a constant number of randomly chosen Pauli measurements to evaluate the process fidelity to a low variance instead of performing a full tomography. However, despite the fact that the mathematical formula of process fidelity as reproduced in Eq. (1) involves Pauli operators as initial states, one cannot directly use Pauli operators as the initial states in experimental settings because Pauli operators are not quantum states. For the sake of satisfying the experimental requirements one could prepare the eigenstates of Pauli operators to be the initial states. An issue with this is that one needs then to prepare eight different initial states for a single qubit (two eigenstates per each Pauli operator). Furthermore, it is also necessary to frequently change the initial states and measurement bases shot by shot, and the efficiency of this change relies on the speed of the device used. For that reason, the zero-fidelity protocol uses symmetric, informationally complete (SIC) states [4] instead of Pauli eigenstates. The four SIC-states can be used directly as initial states because they are quantum states and require just four different initial states for a single qubit. This implies fewer experimental settings in terms of initial states and measurement bases that are needed in order to estimate the process fidelity [2].

It is not easy to characterize SPAM errors experimentally. Therefore, it is important for protocols to be robust to SPAM errors. If unable to characterize SPAM errors, especially when the effect of SPAM errors happens to be large, one may obtain a fidelity evaluation that does not correspond to the actual state of the channel in question. For example, when preparing an initial state, the state may be subject to overrotation errors (state preparation errors). Additionally, when the state is measured, it may flip (e.g., $|0\rangle \rightarrow |1\rangle$) with a certain probability (measurement errors). Furthermore, the higher the number of qubits in a system, the more serious SPAM errors become as more qubits have the potential to get overrotated and more outcomes can flip.

This paper is structured as follows. In Section II, we introduce the zero-fidelity protocol including the SIC-states. In Section III, we present the randomized benchmarking protocol [5–7] and combine it with the zero-fidelity protocol in such a way that the zero-fidelity becomes robust to SPAM errors for systems of up to three qubits. In order to make the zero-fidelity robust to SPAM errors and, at the same time, scalable to larger systems, we apply the zero noise extrapolation method, which is a method for scaling channel noise [8]. Section IV presents experimental results. Section V concludes.

A. Contributions

In this work, we make the following contributions:

* d13222001@ntu.edu.tw
† Corresponding author; renata.wong@cgu.edu.tw
‡ goan@phys.ntu.edu.tw

- We show that the zero-fidelity can be made robust to SPAM errors by being combined with randomized benchmarking. As randomized benchmarking is limited essentially to systems of up to three qubits, this limits then the zero-fidelity also to three qubits.
- We combine the zero-fidelity protocol with zero noise extrapolation method to make it robust to SPAM errors for systems larger than three qubits.
- Through numerical experiments, we demonstrate that combining the zero-fidelity with either randomized benchmarking or zero noise extrapolation indeed is robust to SPAM errors. The results also confirm that such a combination doesn't distort the zero-fidelity, which remains a good approximation to process fidelity.
- The practical implication of our results is that the zero-fidelity has the potential to be used for multi-qubit systems with less experimental resources and at the same time be robust to SPAM errors.

II. ZERO-FIDELITY AS AN APPROXIMATION TO PROCESS FIDELITY

In this section we briefly introduce symmetric, informationally complete (SIC) states [4] and the process fidelity. The zero-fidelity is the zeroth-order approximation to the process fidelity among the k-fidelities described in [2], with the level of accuracy increasing with the increasing order. The SIC-states (a total of four) will be used for state preparation in the zero-fidelity protocol. As opposed to that, the process fidelity uses the density matrices prepared by the eigenstates of Pauli operators for state preparation [9].

The process fidelity is given as

$$F(\Lambda,\Gamma)=\frac{1}{4^n}\sum_{i}^{4^n}\mathbf{Tr}[\Lambda(P_i)\Gamma(P_i)], \tag{1}$$

where P_i ranges over the set of Pauli operators and Λ and Γ are an ideal channel and an actual channel, respectively. The zero-fidelity protocol proposed in [2] approximates the process fidelity, albeit without considering SPAM errors. Here, we will augment the zero-fidelity to account for SPAM errors. To verify the accuracy of our augmentation procedure, we compare the obtained results with those in which SPAM errors were not considered.

A. Symmetric, informationally complete states

According to quantum theory, positive operator valued measures (POVM) are used to perform measurements on quantum systems. A POVM is a set of m positive semidefinite operators $\{E_i\}_{i=1}^m$ that span Hilbert space $\mathcal{H}$ of dimension $d=2^n$, where n is the number of qubits in the system. Those operators must satisfy the requirement of their sum adding up to identity:

$$\sum_{i=1}^{m}E_i=I.$$

Therefore, for a single qubit, one can use the Pauli group as a set of POVMs, $P_i\in\{I,X,Y,Z\}$, while for n qubits, the set of POVMs will be the tensor product of the Pauli operators, $P_i\in\{I,X,Y,Z\}^{\otimes n}$. For $n=1$ there is also another set of operators that can span a d-dimensional Hilbert space $\mathcal{H}$ with a minimal number of elements $d^2=4$. These are the four SIC-states. However, these states are not like Pauli operators, which are mutually orthogonal, i.e.

$$\begin{cases}\mathbf{Tr}[P_iP_j]=0, & \text{if } i\neq j\\ \mathbf{Tr}[P_iP_j]=1, & \text{if } i=j\end{cases}$$

where $P_i\in\{X,Y,Z\}$.

According to [4], the transitional probabilities between the four SIC-states are equal to

$$|\langle\psi_i|\psi_j\rangle|^2=\frac{1}{d+1},\quad i\neq j.$$

That is, no matter what the initial state is, it can always be projected onto the remaining three states with the same probability. This set of POVMs is called *symmetric, informationally complete states* POVM (SIC-POVM). For a single qubit, the four SIC-states are defined as

$$\begin{aligned}|\psi\rangle_1&=|0\rangle\\ |\psi\rangle_2&=\frac{1}{\sqrt{3}}|0\rangle+\sqrt{\frac{2}{3}}|1\rangle\\ |\psi\rangle_3&=\frac{1}{\sqrt{3}}|0\rangle+\sqrt{\frac{2}{3}}e^{i\frac{2\pi}{3}}|1\rangle\\ |\psi\rangle_4&=\frac{1}{\sqrt{3}}|0\rangle+\sqrt{\frac{2}{3}}e^{i\frac{4\pi}{3}}|1\rangle\\ |\langle\psi_i|\psi_j\rangle|^2&=\frac{1}{3},\quad i\neq j\end{aligned}$$

On the Bloch sphere, these states form a regular tetrahedron. It is worth noting that together the four SIC-states are a quantum state 2-design [10, 11].

B. Process fidelity and zero-fidelity

The process fidelity is defined as the overlap between ideal channel and actual channel. In other words, the process fidelity checks how close the ideal quantum operation and the actual quantum operation are. Consider an ideal channel Λ (here we use the same notation as [2]) which maps the initial state ρ_I to the desired final state

$\rho_F = \Lambda(\rho_I)$, and an actual channel Γ which will usually not perfectly match the ideal channel Λ. We can represent the similarity between the ideal channel Λ and the actual channel Γ with the following equation (after [2, 9])

$$F(\Lambda, \Gamma) = \frac{1}{4^n} \sum_{i=1}^{4^n} \mathbf{Tr}[\Lambda(\sigma_i^\dagger)\Gamma(\sigma_i)], \tag{2}$$

where $\sigma_i \in P_i$ is a Pauli operator. Here, we do not normalize Pauli operators so the maximum fidelity is 2^n instead of 1. However, the process fidelity in Eq. (2) cannot be evaluated experimentally because in order to be able to do so the input state must be a quantum state, which means that it can be represented by a density matrix, which is Hermitian, positive-semidefinite and has unit trace, i.e. $\mathbf{Tr}[\rho] = 1$. σ_i is not a quantum state since Pauli operators are traceless. In order to estimate the process fidelity one needs to rewrite Eq. (2) to satisfy this experimental requirement that the input must be a quantum state. With this, the process fidelity is subsequently defined as

$$F(\Lambda, \Gamma) = \frac{1}{4^n} \sum_{i,j=1}^{4^n} [B^{-1}]_{ij} \mathbf{Tr}[\Lambda(\rho_i)\Gamma(\rho_j)], \tag{3}$$

where $B_{ij} = \mathbf{Tr}[\rho_i^\dagger \rho_j]$ checks the overlap between the state ρ_i and the state ρ_j and performs normalization. It is worth noting that if the density matrices ρ_i are prepared by the eigenstates of Pauli operators then the coefficient

$$\begin{cases} B_{ij} = 2^n, & \text{if } i = j \\ B_{ij} = 0, & \text{if } i \neq j. \end{cases}$$

By [9], Eq. (3) will then reduce to

$$F(\Lambda, \Gamma) = \frac{1}{4^n} \sum_{i,j=1}^{4^n} 2^{-n} \mathbf{Tr}[\Lambda(\rho_i)\Gamma(\rho_i)]. \tag{4}$$

From Eq. (3) and in agreement with Born's rule, the term $\mathbf{Tr}[\Lambda(\rho_i)\Gamma(\rho_j)]$ can be considered to be the expectation value of the observable $\Lambda(\rho_i)$ with respect to the final state $\Gamma(\rho_j)$. The final state is obtained by evolving the initial state ρ_j by the actual channel Γ. In the theoretical view, Eq. (3) seems reasonable because the inputs are quantum states and the goal of estimating the process fidelity is to learn how close the ideal and the actual quantum operations are to each other. Nevertheless, Eq. (3) is not practical for measuring the expectation values of observables $\Lambda(\rho_i)$ experimentally because, for most channels Λ and initial states ρ_i, the observables $\Lambda(\rho_i)$ have entangled eigenstates [2].

The reason why one doesn't want observables with entangled eigenstates is that entangled eigenstates cannot be separated. In other words, they cannot be described by a tensor product of individual qubit states, and as such cannot therefore be measured separately. By allowing observables with entangled eigenstates, the entire system would need to be measured together, which is often difficult or impossible to do in practice.

In order to estimate the process fidelity experimentally, Eq. (3) should be rewritten as

$$F(\Lambda, \Gamma) = \frac{1}{4^n} \sum_{i,l}^{4^n} C_{il} \mathbf{Tr}[\Gamma(\rho_i)W_l], \tag{5}$$

with

$$C_{il} = \sum_{j=1}^{4^n} [B^{-1}]_{ji} \mathbf{Tr}[\Lambda(\rho_j)W_l],$$

where W_l is a set of Pauli operators $\{I, X, Y, Z\}^{\otimes n}$. The derivation of this formula is given in Appendix A.

Eq. (5) is not scalable because one needs to prepare 4^n initial states and 4^n observables for measurements. That is, we have to use a total of 16^n experimental settings to estimate the process fidelity experimentally. A way to expedite this is given in [1], where the authors show that one can use joint probability distribution to sample a small subset of initial states and observables instead. This means that the experimental resources needed for estimating the process fidelity can be significantly reduced.

In order to use the protocol in [1] and not to be forced to frequently change initial state and measurement basis one can use the zeroth-order approximation to process fidelity called the zero-fidelity. The zero-fidelity is given as

$$F_0(\Lambda, \Gamma) = \frac{1}{4^n} \sum_{i,j}^{4^n} \mathbf{Tr}[\Lambda(\rho_i)W_j] \mathbf{Tr}[\Gamma(\rho_i)W_j], \tag{6}$$

where ρ_i are prepared by the four SIC-states and W_j are Pauli operators. Nevertheless, the zero-fidelity doesn't take the effects of state preparation and measurement errors into account [2]. Here, we will remedy that while using Eq. (6) to estimate the zero-fidelity [12].

III. ZERO-FIDELITY RANDOMIZED BENCHMARKING AND CHANNEL NOISE SCALING

In this section we will first introduce the randomized benchmarking protocol [5–7] and combine it with the zero-fidelity to make the zero-fidelity robust to SPAM errors. After that, we will use a channel noise scaling method called *zero noise extrapolation* to make the zero-fidelity robust against SPAM errors. The results of our numerical experiments are presented in Section IV.

Based on the randomized benchmarking protocol [13], the process fidelity can be made robust to SPAM errors by applying quantum operations of the noisy and noiseless channels m times and gradually increasing the value

of m. Therefore the process fidelity equation can be written in the following form

$$F^m(\Lambda,\Gamma)=\frac{1}{4^n}\sum_{i=1}^{4^n}\mathbf{Tr}[\Lambda^m(\sigma_i^\dagger)\Gamma^m(\sigma_i)], \tag{7}$$

where σ_i is the tensor product over single-qubit Pauli operators. However, as mentioned in Section II, Eq. (7) cannot be estimated experimentally because Pauli operators are traceless. Instead, one needs to prepare the eigenstates of Pauli operators and avoid using observables $\Lambda(\rho_i)$ with entangled eigenstates. For the above reasons, Eq. (7) is further rewritten as

$$F^m(\Lambda,\Gamma)=\frac{1}{4^n}\sum_{i,j=1}^{4^n}2^{-n}\mathbf{Tr}[\Lambda^m(\rho_i)W_j]\mathbf{Tr}[\Gamma^m(\rho_i)W_j].$$

Based on the reasoning in both randomized benchmarking and cycle benchmarking [9, 13], one can also decouple SPAM errors from the zero-fidelity. In such a scenario, the equation becomes

$$F_0^m(\Lambda,\Gamma)=\frac{1}{4^n}\sum_{i,j=1}^{4^n}\mathbf{Tr}[\Lambda^m(\rho_i)W_j]\mathbf{Tr}[\Gamma^m(\rho_i)W_j]. \tag{8}$$

A. Randomized benchmarking and the process fidelity

We now demonstrate how to combine the process fidelity and randomized benchmarking to obtain the process fidelity for different Clifford lengths m. By different Clifford lengths m we mean that a channel is applied consecutively m times:

$$F^m(\mathcal{U},\tilde{\mathcal{U}})=\frac{1}{4^n}\sum_{i=1}^{4^n}\mathbf{Tr}[\mathcal{U}^m(\rho_i),\tilde{\mathcal{U}}^m(\rho_i)] \tag{9}$$

where $\mathcal{U},\tilde{\mathcal{U}}$ are ideal channel and noisy channel, respectively, and ρ_i are quantum states prepared by the eigenstates of Pauli operators.

A quantum state ρ that evolves through an ideal channel $\mathcal{U}$ can be described as

$$\rho\to\mathcal{U}(\rho)=U\rho U^\dagger,$$

Similarly, a quantum state that evolves through a noisy channel can be described as

$$\rho\to\tilde{\mathcal{U}}(\rho)=\tilde{U}\rho\tilde{U}^\dagger. \tag{10}$$

Assume that the noisy channel $\tilde{\mathcal{U}}$ can be decomposed into $\Lambda\mathcal{U}$ so that Eq. (10) becomes

$$\rho\to\tilde{\mathcal{U}}(\rho)=\Lambda(U\rho U^\dagger).$$

Therefore, from the process fidelity we have

$$F(\mathcal{U},\tilde{\mathcal{U}})=\frac{1}{4^n}\sum_{i=1}^{4^n}\mathbf{Tr}[\rho_iU^\dagger\Lambda(U\rho_iU^\dagger)U].$$

Now, we consider ideal channels and noisy channels applied to a quantum state m times, which we define as

$$\rho_i'=\tilde{\mathcal{C}}^m\rho_i=\Lambda\mathcal{U}^{-1}\Lambda\mathcal{U}_m...\Lambda\mathcal{U}_2\Lambda\mathcal{U}_1\rho_i$$

and

$$\rho_i'=\mathcal{C}^m\rho_i=\mathcal{U}^{-1}\mathcal{U}_m...\mathcal{U}_2\mathcal{U}_1\rho_i,$$

where $\mathcal{U}^{-1}=(\mathcal{U}_m...\mathcal{U}_2\mathcal{U}_1)^{-1}$.

Using the superoperator representation $\Lambda\to\hat{\Lambda}=\sum_k A_k\otimes A_k^*$ and $U\to\hat{U}=U\otimes U^*$ we obtain the process fidelity as

$$\begin{aligned}F(\mathcal{C}^m,\tilde{\mathcal{C}}^m)&=\frac{1}{4^n}\sum_{i=1}^{4^n}\mathbf{Tr}[\mathcal{C}^m(\rho_i)\tilde{\mathcal{C}}^m(\rho_i)]\\&=\frac{1}{4^n}\sum_{i=1}^{4^n}\mathbf{Tr}[\rho_i(\hat{U}_m^{-1}\hat{\Lambda}_m\hat{U}_m\cdots\hat{U}_1^{-1}\hat{\Lambda}_1\hat{U}_1)\rho_i].\end{aligned}$$

From $\mathbb{E}_U(F_g)=\mathbf{Tr}\big[\rho(\int_{U(D)}dU\hat{U}\hat{\Lambda}\hat{U}^{-1})\rho\big]$ (the gate fidelity over all unitary operators by Haar measurement [13]) we obtain the formula for averaging over the Haar measure for the unitary operators

$$\begin{aligned}F_{avg}(\mathcal{C}^m,\tilde{\mathcal{C}}^m)&=\mathbb{E}_U(F(\mathcal{C}^m,\tilde{\mathcal{C}}^m))\\&=\int_{U(D^{\otimes n})}(\Pi_{j=1}^m dU_j)(F(\mathcal{C}^m,\tilde{\mathcal{C}}^m))\\&=\frac{1}{4^n}\sum_{i=1}^{4^n}\mathbf{Tr}(\rho_i\Lambda[\Pi_{j=1}^m\hat{\Lambda}_j^{avg}]\rho_i),\end{aligned}$$

where dU_j denotes the Haar measure and

$$\hat{\Lambda}_j^{avg}\equiv\mathbb{E}_{U_j}(\hat{\Lambda}_j)\equiv\int_{U(D)}dU\hat{U}_1^{-1}\hat{\Lambda}_1\hat{U}_1.$$

As given in [14],

$$\hat{\Lambda}_j^{avg}\rho=p_j\rho+(1-p_j)\frac{\mathbb{I}}{D}$$

with

$$p_j=\frac{\mathbf{Tr}(\hat{\Lambda}_j)-1}{D^2-1}. \tag{11}$$

With the above, we can finally obtain the relation

$$\begin{aligned}F^m(\mathcal{U},\tilde{\mathcal{U}})&=\frac{1}{4^n}\sum_{i=1}^{4^n}\mathbf{Tr}[\mathcal{U}^m(\rho_i)\tilde{\mathcal{U}}^m(\rho_i)]\\&=A_0p^m+B_0,\end{aligned} \tag{12}$$

where the coefficients A_0 and B_0 absorb SPAM errors and the strength of depolarizing error p can be considered as the parameter for the average gate fidelity $F_{ave} = p + \frac{1-p}{2^n}$. Here, we assume the same strength p_j as in Eq. (11), gate-independence and time-independence [13, 15]. See Appendix C for an analysis of the physical meaning of the parameter p.

Now, from [1] one can also estimate the process fidelity by the following equation

$$F^m(\mathcal{U},\tilde{\mathcal{U}}) = \frac{1}{4^n}\sum_{i,j=1}^{4^n} 2^{-n}\mathbf{Tr}[\mathcal{U}^m(\rho_i)W_j]\mathbf{Tr}[\tilde{\mathcal{U}}^m(\rho_i)W_j], \tag{13}$$

where the quantum states ρ_i are prepared by the eigenstates of Pauli operators.

B. Randomized benchmarking and the zero-fidelity

Since the zero-fidelity is not robust to SPAM errors, we will combine it now with randomized benchmarking. This will make it robust to SPAM errors, in addition to being scalable experimentally. From Eq. (13) we can write down the equation for the zero-fidelity as

$$F^m(\mathcal{U},\tilde{\mathcal{U}}) = \frac{1}{4^n}\sum_{i,j=1}^{4^n} \mathbf{Tr}[\mathcal{U}^m(\rho_i)W_j]\mathbf{Tr}[\tilde{\mathcal{U}}^m(\rho_i)W_j], \tag{14}$$

where the quantum states ρ_i are prepared by the SIC-states instead of the eigenstates of Pauli operators. From the discussion above it follows that the form of the zero-fidelity in Eq. (14) is robust to SPAM errors. See Appendix B for the derivation.

In Section IV, we compare the regular randomized benchmarking protocol with the zero-fidelity protocol combined with randomized benchmarking. To that end, we consider two-qubit and three-qubit randomized benchmarking. We use Gottesman–Knill theorem [16], which is an efficient method for obtaining the inverse of the first m Clifford operators to generate the randomized benchmarking circuits [17]. In our circuit, we use Qiskit's [18] noise model of a real backend to add depolarizing noise on every gate and also readout error on the measurement gates. Admittedly, one could just use m Clifford operators to represent Clifford length m. However, in the present work, following Qiskit's `randomized_benchmarking_seq` function, we use a sequence of Clifford operators to represent a single Clifford operator. We do that in order to reduce the number of gate types, namely we restrict the gates to the Hadamard, phase gate and CNOT gates, plus the gates of the Pauli group. Such a reduction has the double benefit of being easily implementable on real devices and that of memory optimization. Namely, it has been shown in [19] that the 92897280-element 3-qubit Clifford group is the semidirect product of the, much smaller, 1451520-element 3-qubit symplectic group with the Pauli group.

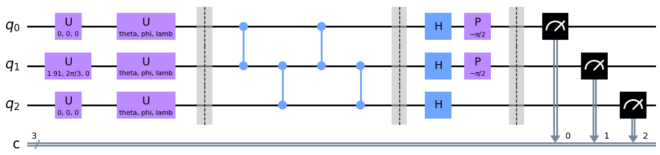


FIG. 1: An example three-qubit circuit. The first U gate on each qubit is for state preparation, where we rotate $|0\rangle$ to one of the SIC-states. The second U gate on each qubit is state preparation error. The actual target channel consists of a block of CZ gates. The gates behind the CZ gates are for performing measurement basis changes. We also add readout error on each measurement gate. The ideal target channel contains no SPAM or gate errors.

This means that one can reconstruct the entire Clifford group by storing just the symplectic group in memory.

C. Channel noise scaling

We first combined the zero-fidelity with randomized benchmarking. However, due to the limitations of the randomized benchmarking protocol with respect to system size, it is difficult to apply the zero-fidelity randomized benchmarking protocol to more than three qubits. This realization led us to a different attempt at making the zero-fidelity robust to SPAM errors. Namely, in order to be able to apply the zero-fidelity to a larger number of qubits, we used channel noise scaling instead of randomized benchmarking. Channel noise scaling refers to a class of methods that adjust the level of noise present in individual channels of a system. The method we used is called *zero noise extrapolation*, or ZNE for short [8].

As an example, let's assume that we want to calculate the zero-fidelity of a channel $\mathcal{U}$ whose circuit looks like the one given in Fig. 1. In Fig. 1, the first U gate on each qubit is for state preparation, where we rotate $|0\rangle$ to one of the SIC-states. The second U gate on each qubit is a state preparation error. Then follows the actual target channel, which contains a block of CZ gates. The gates behind the CZ gate block are for performing measurement basis changes. We also add readout error on each measurement gate.

We can apply the same channel $\mathcal{U}$ a number m times, i.e. $(\mathcal{U}\mathcal{U}^\dagger)^m = \mathcal{I}^m$, where $m \geq 1$. This method is called *global folding* [8]. By applying global folding to the circuit in Fig. 1, we effectively extend only the CZ block of the circuit m times. The gates before the block as well as the gates after the block remain intact. So, for $m = 1$, the circuit will consist of a CZ block containing a total of 8 CZ gates, while for $m = 2$, the circuit will have a block of 16 CZ gates, etc. This method produces a total of $m + 1$ circuits for a given m.

In the ideal case, repeatedly applying the same circuit will not affect the final result. However, the error will increase with the number of channels applied in actual experiments. This indicates that the zero-fidelity can be seen as a function of the number of circuits. With this,

one can then also obtain a decay rate by fitting the results of the zero-fidelity against the number of circuits.

Repeatedly applying identity circuits, also known as *identity folding*, has been used for mitigating errors in quantum computation for instance in [8, 20, 21]. It has been shown experimentally that if the noise is depolarizing noise (and this holds also in the case of gate-dependence) the results can be fitted with the same exponential decay as in randomized benchmarking [8]. Using this method, we don't have to choose Clifford gates randomly from the Clifford group in order to calculate the average gate fidelity. Instead, we can obtain a fidelity value from the zero-fidelity decay rate, and this value will be independent of SPAM errors. Since we don't need to choose from the Clifford gates, we do not therefore need to deal with the high number of Clifford elements in the Clifford group. This implies the ability to obtain the zero-fidelity for systems of more than three qubits as well.

In the following section, we demonstrate how to make the zero-fidelity independent of SPAM errors and perform simulations on systems of up to five qubits.

IV. NUMERICAL RESULTS

Our simulation results include estimations of the zero-fidelities alone (Section IV A), as well as of the zero-fidelities in combination with randomized benchmarking or zero noise extrapolation (Sections IV B and IV C, respectively).

A. Zero-fidelity without SPAM error robustness

Here, we present our numerical results for the zero-fidelity estimation on three qubits. The results include estimations under both noisy and noiseless channels.

When estimating the zero-fidelity for the noisy channel with CZ gates, as shown in Fig. 1, we model the SPAM errors as rotation errors sampled from a Gaussian distribution for state preparation, and as readout errors for measurement. The readout errors we apply include both strong and weak readout errors defined below:

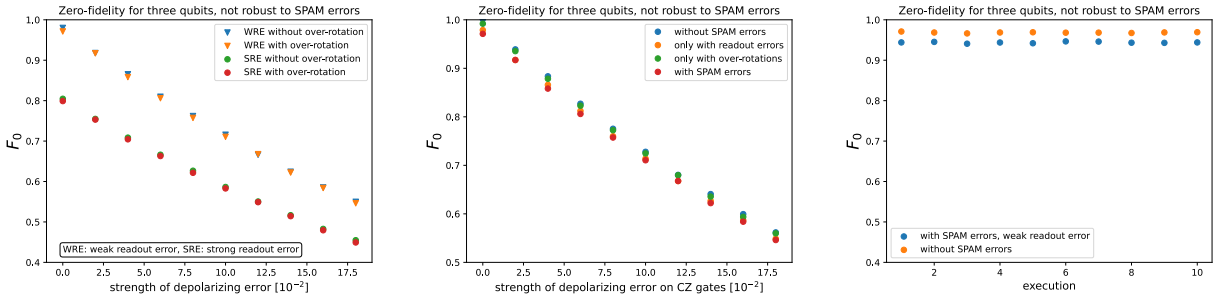
$$\text{strong readout error} = \begin{pmatrix} 0.997 & 0.003 \\ 0.005 & 0.995 \end{pmatrix} \tag{15}$$

$$\text{weak readout error} = \begin{pmatrix} 0.97 & 0.03 \\ 0.05 & 0.95 \end{pmatrix}. \tag{16}$$

The strength of the strong readout error is 10 times that of the weak readout error. Fig. 2c shows the fidelities of the channels mentioned above either with or without SPAM errors and a fixed gate error. We use Qiskit's [18] noise model to create a depolarizing channel whose mathematical form can be written as

$$E(\rho) = (1-\lambda)\rho + \lambda \mathbf{Tr}[\rho]\frac{\mathbf{I}}{2^n}, \tag{17}$$

where ρ are the SIC-states, n is the number of qubits and λ is the gate error fixed to 0.01 in our experiments.



(a) Strong vs weak readout errors. Varying depolarizing error.

(b) Varying depolarizing error strength, and weak readout error.

(c) Fidelity at fixed gate error $\lambda = 0.01$.

FIG. 2: Zero-fidelity for three-qubit circuit as in Fig. 1.

The zero-fidelities of the target circuit in Fig. 1 are estimated in ten experiments with and without SPAM errors. Each experiment consisted of a total of 4096 different circuits. This number reflects all the possible combinations of state preparation gates and measurement bases. There are four different SIC states and four measurement bases. Consequently, for three qubits there are a total of 4^3 possible combinations of state preparations and 4^3 possible combinations of measurement bases.

The results are shown in Fig. 2. In Fig. 2a the gate error is the depolarizing error on CZ gates. We compare the fidelities under the weak readout error and the strong readout error. The over-rotations are sampled from the Gaussian distribution. The outcome is the zero-fidelity

F_0 and the values are as expected, that is, stronger readout errors and increasing strength of the depolarizing error lead to lower fidelity values. Presence of over-rotations contributes to the overall value but is not as significant as the readout or depolarizing error.

In Fig. 2b we also consider the effect on zero-fidelity with increasing depolarizing error on CZ gates. Here, we compare four scenarios: without any SPAM errors; only with weak readout error but no over-rotations; only over-rotations without readout errors; and with SPAM errors that include both over-rotations and the weak readout error. The degrees of over-rotation error are sampled from the Gaussian distribution (with zero mean and $\sqrt{5}$ standard deviation) so that each of the 4096 circuits has a different degree of rotation. Here too, the results show a significant impact of the depolarizing noise on the zero-fidelity. Executions without any SPAM errors resulted in consistently higher fidelities than executions with all possible SPAM errors or with some of the SPAM errors.

In Fig. 2c, the degrees of rotation are sampled from the Gaussian distribution with mean $\mu = 0$ and standard deviation $\sigma = \sqrt{5}$, and the readout error is described by the matrix in Eq. (15). In both cases, with and without SPAM errors, a constant depolarizing noise was added on the CZ gates. For all executions the parameter λ in Eq. (17) was fixed to 0.01. The average zero-fidelity without SPAM errors was 0.968, while the average zero-fidelity with SPAM errors was 0.943.

B. Zero-fidelity with randomized benchmarking

This section presents the numerical results obtained from combining the zero-fidelity with randomized benchmarking (RB).

The way we combine zero-fidelity with randomized benchmarking is as follows:

1. Apply a sequence of $m+1$ operators chosen uniformly from the Clifford group. The first m operators can be chosen randomly, however the choice of the $(m+1)$-th operator depends on the first m operators because the $(m+1)$-th operator is the inverse of all the other m operators taken together. Formally, let C be an operator and let $S = C_{m+1} \circ C_m \circ ...C_3 \circ C_2 \circ C_1$, where $\circ$ denotes composition of operators. Then we require that $C_{m+1} = (C_m \circ ...C_3 \circ C_2 \circ C_1)^{-1}$. If the operators are ideal (i.e., no noise is present), the sequence applied onto the quantum state is $S(\rho) = \rho$. For a noisy quantum operator $\tilde{C} = \Lambda \circ C$ and a sequence $\tilde{S}$, we can describe them as $\tilde{S}_m = \bigcirc_{j=1}^{m+1}(\Lambda \circ C_j)$. Here, we generate more than one sequence $\tilde{S}_{l_m} = \bigcirc_{j=1}^{m+1}(\Lambda \circ C_{l_j})$ and then apply all of the generated sequences on the initial states. An example circuit for two-qubit systems is given in Fig. 3.

2. For each sequence calculate the expectation values of Pauli operators W_j with respect to the final states $S_{l_m}(\rho_i)$ and $\tilde{S}_{l_m}(\rho_i)$, respectively, where ρ_i are the initial states, i.e. the SIC-states. After that, calculate the overlap as follows:

$$\frac{1}{4^n}\sum_{i,j}^{4^n} \mathbf{Tr}[S_{l_m}(\rho_i)W_j]\mathbf{Tr}[\tilde{S}_{l_m}(\rho_i)W_j] \tag{18}$$

3. Estimate Eq. (18) for different sequence l and different Clifford length m and then average the random sequence to find the averaged sequence fidelity:

$$F^m_{seq}(\mathcal{S}^m, \tilde{\mathcal{S}}^m) = \frac{1}{4^n}\sum_{i,j}^{4^n} \mathbf{Tr}[\mathcal{S}^m(\rho_i)W_j]\mathbf{Tr}[\tilde{\mathcal{S}}^m(\rho_i)W_j], \tag{19}$$

where

$$\mathcal{S}^m = \frac{1}{L}\sum_{l=1}^{L} S^m_l.$$

4. Use the results estimated using Eq. (19) to fit the model mentioned above:

$$F^m_{seq}(\mathcal{S}^m, \tilde{\mathcal{S}}^m) = A_0 p^m + B_0.$$

5. With the result from Step 4 plot the exponential decay curve of the process fidelity and Clifford length m.

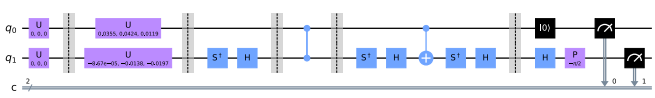


FIG. 3: A simple example a two-qubit circuit for zero-fidelity combined with interleaved randomized benchmarking. The first block of U gates is for preparation of SIC states, the second block of U gates is the state preparation error. Then, we have a Clifford gate represented by two operations, followed by the interleaved CZ channel, and the inverse of the Clifford gate. The gates directly before the measurements are used for basis change. For regular randomized benchmarking, we don't consider the interleaved CZ channel.

For randomized benchmarking, one can consider systems of up to three qubits. Here, we estimate the zero-fidelity with randomized benchmarking on circuits of two and three qubits. We set $l = 5$, and there were a total of $4^n \times 4^n$ circuits per run, where n is the system size.

The numerical results are shown in Fig. 4. All fidelity values were obtained under presence of depolarizing error. Fig. 4a is for systems of two qubits and shows the decay of the zero-fidelity as a function of Clifford number m with and without SPAM errors. One can observe that the zero-fidelity is affected by SPAM errors. However, with an increasing m, the effect of those errors decreases. The values of the zero-fidelity converge to the same value when m is large. The curves are fitted using the values of the zero-fidelity and the equation $F^m = A_0 p^m + B_0$.

For each of the fitted curves we obtained statistics consisting of the decay rate p, the average gate fidelity $F_{\mathbf{ave}}$, and the average error rate r. The average error rate is $r \equiv 1 - F_{\mathbf{ave}}$ [22]. The average gate fidelity is calculated following [13, 23] as $F_{\mathbf{ave}} = p + (1-p)/2^n$.

The statistics are shown in Table I. It is observed that no matter whether there are SPAM errors in the circuit or not, the decay rate of the zero-fidelity will not be affected. This shows that the combination of the zero-fidelity with randomized benchmarking is robust to SPAM errors for the two-qubit case.

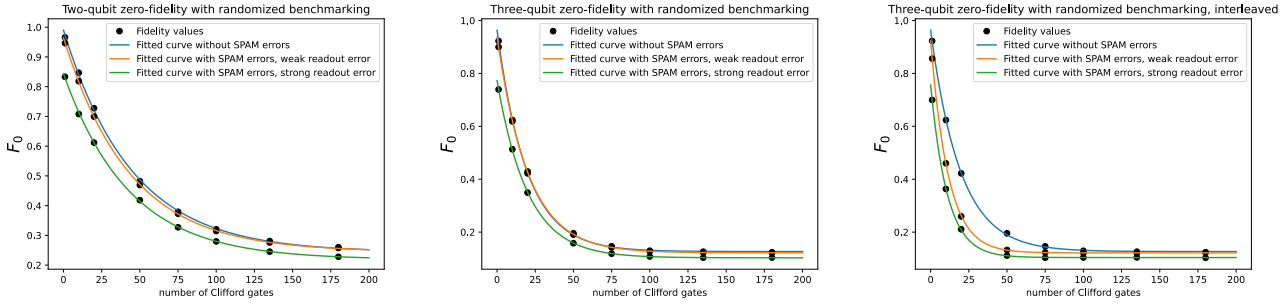
Fig. 4b shows the results for the zero-fidelity with randomized benchmarking on three-qubit systems. The statistics for this experiment are given in Table II. Similarly to Fig. 4a, the values of the zero-fidelity almost converge to the same value when m is large. Also, as it was the case for two-qubit zero-fidelity with randomized benchmarking, no matter whether there are SPAM errors or not, the decay rate of the zero-fidelity will not be affected. This shows that, for the three-qubit case as well, the combination of the zero-fidelity with randomized benchmarking is robust to SPAM errors.

For the last experiment, we used circuits with three qubits too, but we interleaved the target circuit (Fig. 1) into the randomized benchmarking protocol. This method is called *interleaved randomized benchmarking* [24, 25]. The results of estimating zero-fidelity using interleaved randomized benchmarking are shown in Fig. 4c. The blue curve was obtained from fidelity values that involved no interleaving because we needed to calculate the original zero-fidelity with randomized benchmarking for comparison. The curves involving SPAM errors were obtained from the zero-fidelity with interleaved randomized benchmarking.

TABLE I: Statistics for the zero-fidelity with randomized benchmarking on two-qubit systems.

Curve[a]	Decay rate p	Avg. error r[b]	$F_{\mathbf{ave}}$
w/o SPAM err.	0.977	$1.71 \cdot 10^{-2}$	0.983
SPAM err., WRE	0.977	$1.71 \cdot 10^{-2}$	0.983
SPAM err., SRE	0.977	$1.71 \cdot 10^{-2}$	0.983

[a] WRE: weak readout error. SRE: strong readout error
[b] Avg. error per Clifford gate



(a) Two-qubit system.

(b) Three-qubit system.

(c) Three-qubit system. Only circuits with SPAM errors were interleaved.

FIG. 4: Zero-fidelity with randomized benchmarking.

By calculating the decay rate from each fitted curve for the channel with CZ gates, we obtain the zero-fidelity $F_0 \simeq 0.967$ for both the case without SPAM errors and the two cases with SPAM errors and readout error. This value is nearly equal to the fidelity shown in Fig. 2c. From the above results one can observe that even when the strength of the readout error is increased, the same zero-fidelities of the target circuit are obtained. The curves with SPAM errors are lower than the curve without SPAM errors because we have included some extra gates for interleaved randomized benchmarking. However, they all converge to the same values when the number of Clifford gates is large. Therefore, the results demonstrate that by using randomized benchmarking with zero-fidelity we can calculate the zero-fidelity without the effects caused by SPAM errors.

C. Zero-fidelity with zero noise extrapolation

In this section, we show the results for the zero-fidelity for more than three-qubit systems by using the zero noise extrapolation method. This method is realized by global unitary folding, which involves repeatedly applying the identity layers of the quantum circuit (identity scaling).

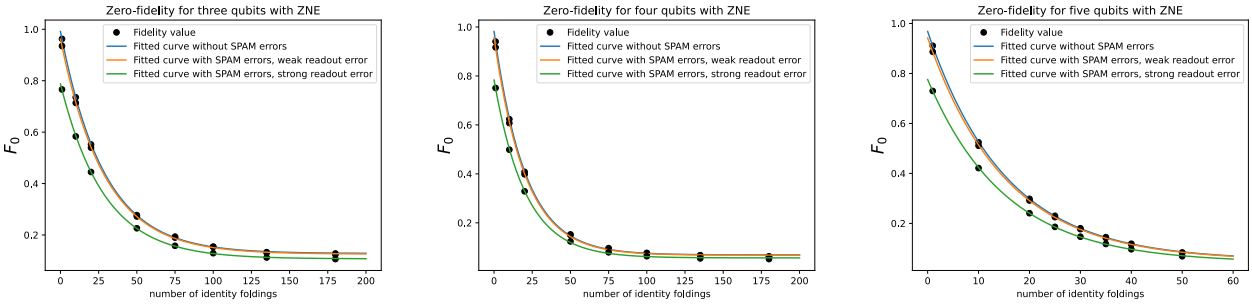
We consider quantum systems with three, four, and five qubits. While calculating the zero-fidelity, we set the parameter $\lambda = 0.01$ for depolarizing noise, see Eq.(17).

Since noise in Qiskit's noise model [18] is added on gates, the zero-fidelity for a depolarizing channel is not just the parameter λ. Rather, the total effect of noise depends on the number of gates in the circuit. Consider for example the circuit in Fig. 1. According to Qiskit's noise model, the depolarizing noise was added on each CZ gate in the channel, so the zero-fidelity calculated the total effect of the depolarizing noise caused by all of those gates, that is, $0.99^4 \approx 0.961$. This is the theoretical value one would obtain mathematically. However, when a measurement is performed, one needs to specify a particular number of shots. Due to the probabilistic character of quantum mechanics, the higher the number of shots, the higher the accuracy. In our experiments, we used 1024 shots, and this has led to a projective error, which can explain the fidelity value we obtained, 0.968, being a bit off from the expected theoretical value of 0.961. For the above reason, the parameter p indicates the strength of the depolarizing channel caused by the total number of gates in our circuit.

TABLE II: Statistics for the zero-fidelity with randomized benchmarking on three-qubit systems.

Curve[a]	Decay rate p	Avg. error r[b]	$F_{\mathbf{ave}}$
w/o SPAM err.	0.952	$4.20 \cdot 10^{-2}$	0.958
SPAM err., WRE	0.952	$4.20 \cdot 10^{-2}$	0.958
SPAM err., SRE	0.952	$4.23 \cdot 10^{-2}$	0.958

[a] WRE: weak readout error. SRE: strong readout error
[b] Avg. error per Clifford gate



(a) $p \simeq 0.966$ for all curves. (b) $p \simeq 0.952$ for all curves. (c) $p \simeq 0.937$ for all curves.

FIG. 5: Zero-fidelity with zero noise extrapolation.



(a) Avg. zero-fidelity without SPAM errors: 0.953, avg. zero-fidelity with SPAM errors: 0.914.

(b) Avg. zero-fidelity without SPAM errors: 0.938, avg. zero-fidelity with SPAM errors: 0.890.

FIG. 6: Zero-fidelity for four and five qubits. Depolarizing error was added on CZ gates for the executions with SPAM errors. λ was set to 0.01.

Fig. 5 shows the fitted fidelity curves for systems of three, four, and five qubits, respectively. For all three graphs one can observe that the fidelity values with SPAM errors are lower than the fidelity values without SPAM errors. However, when we fit the curves using these values we obtain the same decay rates no matter whether there were SPAM errors or not, and no matter how strong the SPAM errors were.

For three qubits (Fig. 5a), the parameter p for all three fitted curves was $p \simeq 0.966$, which is almost the same

as the fidelity without SPAM errors calculated by using single circuit length in Fig. 2c. For four qubits (Fig. 5b), the parameter p for all three fitted curves was $p \simeq 0.952$, which almost equals to the fidelity without the effects from SPAM errors in Fig. 6a. For five qubits (Fig. 5c), the parameter p for all three fitted curves was $p \simeq 0.937$, which is almost the same as for the fidelity without SPAM errors in Fig. 6b.

V. CONCLUSION

In this work, we demonstrated how to make the zero-fidelity robust to SPAM errors by combining it with randomized benchmarking and zero noise extrapolation (ZNE). The performed numerical experiments confirm the correctness of our methodology.

Combined with randomized benchmarking, the zero-fidelity can be estimated for systems of up to three qubits. A combination of the zero-fidelity with ZNE, on the other hand, allowed us to perform tests on circuits of up to five qubits. The obtained results indicate that ZNE scales better and requires less resources than the zero-fidelity randomized benchmarking. In randomized benchmarking, one needs to choose Clifford elements randomly from a large-sized Clifford group. For three-qubit systems, there are a total of 92,897,280 Clifford elements in the Clifford group. For five-qubit systems, the number of elements reaches $\simeq 10^{19}$. Randomly choosing from such a large number of elements not only requires a large computer memory to store the elements but also makes the number of circuits that need to be generated and run simulations on very large.

A future work will be to study how to apply such schemes for noise channels other than the depolarizing noise channels, and to investigate other potential efficient and scalable schemes, such as cycle benchmarking [9], to make the zero fidelity independent of SPAM errors.

ACKNOWLEDGMENTS

The authors wish to acknowledge the support of the National Taiwan University's High Performance Computing facilities, on which our numerical results were obtained. Yu-Hao Chen and Renata Wong acknowledge support from the National Science and Technology Council grant No. NSTC 114-2112-M-182-002-MY3. Renata Wong acknowledges support from Chang Gung Memorial Hospital grant No. BMRPL94.

VI. CODE AVAILABILITY

The code used for this paper can be found at `https://github.com/plain12356/RB_with_zero_fidelity`

Appendix A: Another form of the process fidelity

We derive the equation

$$F(\Lambda,\Gamma) = \frac{1}{4^n}\sum_{i,j=1}^{4^n} C_{ij}\mathbf{Tr}[\Gamma(\rho_i)W_j]$$

with $C_{ij} = \sum_{l=1}^{4^n}[B^{-1}]_{li}\mathbf{Tr}[\Lambda(\rho_l)W_j]$ from the equation

$$F(\Lambda,\Gamma) = \frac{1}{4^n}\sum_{i=1}^{4^n}\mathbf{Tr}[\Lambda(\sigma_i^\dagger)\Gamma(\sigma_i)],$$

where W_j is a set of Pauli operators, ρ_i are the quantum states which are prepared by the eigenstates of Pauli operators, and Λ, Γ are the ideal channel and the actual channel, respectively. Before the derivation we introduce some notational conventions.

1. Preliminary notation

We define the vectorization of a matrix, which is a linear transformation converting a matrix into a vector form.

Let A be a $m \times n$ matrix and let $\mathbf{Vec}(A)$ denote a vectorization of the matrix A given as

$$\mathbf{Vec}(A) = [a_{1,1}, ...a_{m,1}, a_{1,2}, ..., a_{m,2}, ..., a_{m,n}]^{\mathbf{T}}$$

, where $\mathbf{T}$ stands for transposition. Here is an example:

$$M = \begin{pmatrix} 1 & 2 \\ 3 & 4 \end{pmatrix} \quad \rightarrow \quad \mathbf{Vec}(M) = \begin{pmatrix} 1 \\ 3 \\ 2 \\ 4 \end{pmatrix}$$

The vectorization of a product of three matrices ABC is given as

$$\mathbf{Vec}(ABC) = (C^{\mathbf{T}} \otimes A)\mathbf{Vec}(B) \tag{A1}$$

and the inner product (Hilbert–Schmidt inner product) between two vectorized matrices is

$$\mathbf{Vec}(A)^\dagger \mathbf{Vec}(B) = \mathbf{Tr}(A^\dagger B).$$

For convenience we denote $\mathbf{Vec}(A) = |A\rangle\rangle$ and $\mathbf{Vec}(A)^\dagger = \langle\langle A|$. Now assume a density matrix ρ that is evolved by a channel $\mathcal{U}$, which can be represented as

$$\rho' \rightarrow \mathcal{U}(\rho) = U\rho U^\dagger,$$

where U is a unitary matrix. Because of equation (A1), ρ' can be rewritten as

$$\begin{aligned} \mathbf{Vec}(\rho') &= \mathbf{Vec}(\mathcal{U}(\rho)) \\ &= \mathbf{Vec}(U\rho U^\dagger) \\ &= (U^\dagger \otimes U)\mathbf{Vec}(\rho) \\ &= \mathcal{U}|\rho\rangle\rangle \end{aligned} \tag{A2}$$

Here we use the superoperator representation to describe the channel $\mathcal{U} = (U^\dagger \otimes U)$. It can be understood that the superoperator $\mathcal{U}$ in term (A2) is an operator and the vectorized ρ is a vector.

2. Derivation

We can now vectorize the Pauli operator

$$P_i \to |P_i\rangle\rangle/\sqrt{2^n},$$

where n is the number of qubits. For $n = 1$ the vectorized Pauli operators can be represented as

$$|P_i\rangle\rangle \in \{|I\rangle\rangle \quad |X\rangle\rangle \quad |Y\rangle\rangle \quad |Z\rangle\rangle\}$$

, where

$$|I\rangle\rangle = \begin{pmatrix}1\\0\\0\\1\end{pmatrix} |X\rangle\rangle = \begin{pmatrix}0\\1\\1\\0\end{pmatrix} |Y\rangle\rangle = \begin{pmatrix}0\\i\\-i\\0\end{pmatrix} |Z\rangle\rangle = \begin{pmatrix}1\\0\\0\\-1\end{pmatrix}$$

Since the density matrix can be represented by the Pauli operator, we represent a quantum state as

$$|\rho\rangle\rangle = \sum_i c_i |P_i\rangle\rangle, \tag{A3}$$

where $c_i = \langle\langle P_i|\rho\rangle\rangle$ (we have normalized Pauli operators in order to avoid the factor). Note that the coefficients c_i can be considered to be the expectation values of Pauli operators with respect to the quantum state ρ. Putting the coefficients c_i back into Eq. (A3), the quantum state becomes

$$|\rho\rangle\rangle = \sum_i |P_i\rangle\rangle\langle\langle P_i|\rho\rangle\rangle. \tag{A4}$$

Consider another quantum state

$$|\sigma\rangle\rangle = \sum_j |P_j\rangle\rangle\langle\langle P_j|\sigma\rangle\rangle. \tag{A5}$$

One can perform the Hilbert–Schmidt inner product to obtain

$$\mathbf{Tr}[\sigma^\dagger\rho] = \sum_i \sum_j \langle\langle\sigma|[P_j\rangle\rangle(\langle\langle P_j|P_i\rangle\rangle)\langle\langle P_i]|\rho\rangle\rangle \tag{A6}$$

$$= \sum_i \langle\langle\sigma|P_i\rangle\rangle \cdot \langle\langle P_i|\rho\rangle\rangle \tag{A7}$$

$$= \sum_{i=1} \mathbf{Tr}[\sigma P_i]\mathbf{Tr}[\rho P_i]. \tag{A8}$$

because Pauli operators are mutually orthogonal, which means that

$$\begin{cases}\mathbf{Tr}[P_iP_j] = 0, & \text{if } i \neq j\\ \mathbf{Tr}[P_iP_j] = 1, & \text{if } i = j\end{cases}$$

and recall that $\langle\langle P_i|\rho\rangle\rangle = \mathbf{Tr}[\rho P_i]$. Now, back to the equation

$$F(\Lambda,\Gamma) = \frac{1}{4^2}\sum_{i=1}^{4^2} \mathbf{Tr}[\Lambda(\sigma_i^\dagger)\Gamma(\sigma_i)],$$

where $\{\sigma_i\}_{i=1}^4$ is a set of Pauli operators, for n qubits $\sigma_i \in \{I, X, Y, Z\}^{\otimes n}$.

We can rewrite

$$F(\Lambda,\Gamma) = \frac{1}{4^n}\sum_{i=1}^{4^n} \mathbf{Tr}[\Lambda(\sigma_i^\dagger)\Gamma(\sigma_i)]$$

as

$$F(\Lambda,\Gamma) = \frac{1}{4^n}\sum_{i,j=1}^{4^n} [B^{-1}]_{ij}\mathbf{Tr}[\Lambda(\rho_i)\Gamma(\rho_j)], \tag{A9}$$

where $B_{ij} = \mathbf{Tr}[\rho_i^\dagger\rho_j]$ and ρ_i, ρ_j are density matrices that can be prepared from the eigenstates of Pauli operators. Let $\rho' = \Lambda(\rho)$ and $\sigma = \Gamma(\rho)$ so Eq. (A9) becomes

$$F(\Lambda,\Gamma) = \frac{1}{4^n}\sum_{i,j=1}^{4^n} [B^{-1}]_{ij}\mathbf{Tr}[\rho_i'\sigma_j]. \tag{A10}$$

From Eqs. (A6) through (A8) we obtain

$$\begin{aligned}F(\Lambda,\Gamma) &= \frac{1}{4^n}\sum_{i,j=1}^{4^n} [B^{-1}]_{ij}\mathbf{Tr}[\rho_i'\sigma_j]\\ &= \frac{1}{4^n}\sum_{i,j=1}^{4^n}\sum_{k=1}^{4^n}[B^{-1}]_{ij}\mathbf{Tr}[\sigma_jP_k]\mathbf{Tr}[\rho_i'P_k]\\ &= \frac{1}{4^n}\sum_{i,j=1}^{4^n}\sum_{k=1}^{4^n}[B^{-1}]_{ij}\mathbf{Tr}[\Gamma(\rho_j)P_k]\mathbf{Tr}[\Lambda(\rho_i)P_k].\end{aligned}$$

As mentioned in the beginning of this appendix, we finally get

$$F(\Lambda,\Gamma) = \frac{1}{4^n}\sum_{i,j=1}^{4^n} C_{ij}\mathbf{Tr}[\Gamma(\rho_i)W_j]$$

with $C_{ij} = \sum_{l=1}^{4^n}[B^{-1}]_{li}\mathbf{Tr}[\Lambda(\rho_l)W_j]$, where W_j is a set of Pauli operators.

Appendix B: Decay rate of the zero-fidelity

We show that the equation

$$F^m(\mathcal{U},\tilde{\mathcal{U}}) = \frac{1}{4^n}\sum_{i,j=1}^{4^n} \mathbf{Tr}[\mathcal{U}^m(\rho_i)W_j]\mathbf{Tr}[\tilde{\mathcal{U}}^m(\rho_i)W_j],$$

where ρ_i are the quantum state prepared by the SIC-states and W_j is a set of Pauli operators, is equal to

$$A_0p^m + B_0, \tag{B1}$$

where the coefficients A_0 and B_0 absorb state preparation and measurement errors, and m is the number of Clifford operators.

Since the process fidelity

$$F(\Lambda,\Gamma)=\frac{1}{4^n}\sum_{i=1}^{4^n}\mathbf{Tr}[\Lambda(\sigma_i^\dagger)\Gamma(\sigma_i)]$$

can be written as follows (this was established in Appendix A)

$$F(\Lambda,\Gamma)=\frac{1}{4^n}\sum_{i=1}^{4^n}\mathbf{Tr}[\Lambda(\rho_i)W_j]\mathbf{Tr}[\Gamma(\rho_i)W_j]$$

we only need to prove that the process fidelity with the channel applied m times, i.e.,

$$F^m(\Lambda,\Gamma)=\frac{1}{4^n}\sum_{i=1}^{4^n}\mathbf{Tr}[\Lambda^m(\sigma_i^\dagger)\Gamma^m(\sigma_i)]$$

is equal to Eq. (B1).

As shown in Section III,

$$\begin{aligned}F^m(\mathcal{U},\tilde{\mathcal{U}})&=\frac{1}{4^n}\sum_{i=1}^{4^n}\mathbf{Tr}[\mathcal{U}^m(\rho_i)\tilde{\mathcal{U}}^m(\rho_i)]\\&=A_0p^m+B_0\end{aligned}$$

. We have also shown that

$$\begin{aligned}F(\Lambda,\Gamma)&=\frac{1}{4^n}\sum_{i=1}^{4^n}\mathbf{Tr}[\Lambda(\sigma_i^\dagger)\Gamma(\sigma_i)]\\&=\frac{1}{4^n}\sum_{i,j=1}^{4^n}C_{ij}\mathbf{Tr}[\Lambda(\rho_i)W_j],\end{aligned}$$

where

$$C_{ij}=\sum_{l=1}^{4^n}[B^{-1}]_{li}\mathbf{Tr}[\Gamma(\rho_i)W_j],\tag{B2}$$

. Furthermore, if the density matrix ρ_i is prepared by the eigenstates of Pauli operators, we can write the process fidelity after [9] as

$$F(\Lambda,\Gamma)=\frac{1}{4^n}\sum_{i,j}^{4^n}2^{-n}\mathbf{Tr}[\Gamma(\rho_i)W_j]\mathbf{Tr}[\Lambda(\rho_i)W_j].\tag{B3}$$

Now let the quantum states be prepared by the SIC-states instead of the eigenstates of Pauli operators. In this case, the coefficient 2^{-n} in Eq. (B3) is 1 and then Eq.(B3) becomes

$$F(\Lambda,\Gamma)=\frac{1}{4^n}\sum_{i,j}^{4^n}\mathbf{Tr}[\Gamma(\rho_i)W_j]\mathbf{Tr}[\Lambda(\rho_i)W_j]$$

Finally, it can be concluded that

$$\begin{aligned}F^m(\Lambda,\Gamma)&=\frac{1}{4^n}\sum_{i,j}^{4^n}\mathbf{Tr}[\Gamma^m(\rho_i)W_j]\mathbf{Tr}[\Lambda^m(\rho_i)W_j]\\&=A_0p^m+B_0\end{aligned}$$

Appendix C: The physical meaning of parameter p in channel noise scaling

In this appendix, we analyze the physical meaning of parameter p. This parameter can be obtained by fitting the results of the zero-fidelity. The decrease in the fidelity is a result of applying quantum circuits repeatedly, i.e., letting channel noise to accumulate. We refer to this method as *identity folding*. First, we introduce complex projective designs.

a. Complex projective t-design

The definition of a complex projective design is similar to the definition of a spherical design. Consider a finite subset of unit vectors $\mathbf{X}$ on a sphere $\mathbf{S}(\mathbb{R}^d)$, where $\mathbb{R}^d$ is d-dimensional Euclidean space. The following is the definition of a spherical t-design based on [26, 27].

Definition C.1 *Let t be a natural number. A finite subset $\mathbf{X}\subseteq\mathbf{S}(\mathbb{R}^d)$ is called a spherical t-design if*

$$\frac{1}{|\mathbf{S}(\mathbb{R}^d)|}\int_{\mathbf{X}\in\mathbf{S}(\mathbb{R}^d)}f(\mathbf{X})d\sigma(\mathbf{X})=\frac{1}{|\mathbf{X}|}\sum_{\mathbf{u}\in\mathbf{X}}f(\mathbf{u})\tag{C1}$$

holds for any polynomial $f(\mathbf{X})=f(x_1,x_2,...,x_n)$ of degree at most t, with the usual integral on the unit sphere.

For complex projective t-design, instead of on the real d-dimensional space $\mathbb{R}^d$, the subset of unit vectors $\mathbf{X}$ is in $\mathbf{S}(\mathbb{C}^d)$. Furthermore the degree of the polynomial function is t, meaning the function has degree at most t for all real numbers in the entries of the vectors and at most t for the complex conjugates of these entries. The definition of complex projective t-design is given below and follows [10].

Definition C.2 *Let $p_{t,t}$ be a polynomial that has homogeneous degree t in d variables, and degree t in the complex conjugates of these variables. It can be written as*

$$\frac{1}{|\mathbf{X}|}\sum_{x\in\mathbf{X}}p_{t,t}(x)=\int_{\mathbf{S}(\mathbb{C}^d)}p_{t,t}(u)d\eta(u)\tag{C2}$$

From Def. (C2) we can see that complex projective designs can be written in terms of quantum states. The reason why complex projective designs can be written in such a way is that quantum states are vectors in a Hilbert space (complex space). The following is the form of complex projective designs in terms of quantum states:

Definition C.3 *Let $\{p_1,p_2,...,p_K\}$ be a probability distribution over quantum states $\{|\psi_1\rangle,|\psi_2\rangle,\ldots,|\psi_K\rangle\}$. Such a distribution is called a quantum state design if*

$$\sum_i p_i(|\psi_t\rangle\langle\psi_t|)^{\otimes t}=\int_\Psi d\Psi(|\Psi\rangle\langle\Psi|)^{\otimes t}.$$

Def. C.3 means that quantum state design is a probability distribution over a finite set of quantum states [10]. From Ref. [28] we know that a unitary t-design induces quantum state t-designs for the probability distribution over states $U|\psi_0\rangle$, where U is chosen from unitary group with fixed state $|\psi_0\rangle$ [29]. The relation between unitary designs and quantum state designs is important to our analysis. The reason is that the four SIC-states are the quantum state 2-design [10, 11] which means that we can make a connection between SIC-states and the unitary 2-design. Therefore, we can sum up the SIC-states with a fixed unitary U.

b. Quantum state design and depolarizing channel

So far we have introduced spherical t-designs, and complex projective t-designs also known as quantum state t-designs. We also mentioned the relationship between quantum state t-designs and unitary t-designs. Since the four SIC-states are quantum state 2-design, we would like to justify that the parameter p obtained by fitting the results of the zero-fidelity (where the initial states are SIC-states) with the method of repeatedly applying circuits (identity folding) has a physical meaning.

Here, we show that the physical meaning of parameter p obtained by fitting the results of the zero-fidelity corresponds to the strength of depolarizing channel. Therefore, with the decay rate we can learn the channel fidelity between an ideal channel and an actual channel without considering the effects from SPAM errors.

We now consider the formula for average gate fidelity

$$\mathbb{E}(F_g) = \int_{U(D)} dU \mathbf{Tr}[\rho U^{-1} \Lambda_{\mathbf{c}}(U\rho U^{-1})U], \tag{C3}$$

where dU is the unitarily invariant Haar measure, ρ is a quantum state $|\psi\rangle\langle\psi|$ and $\Lambda_{\mathbf{c}}$ is a noisy channel. Eq. (C3) means that the gate fidelity is averaged over the unitary group. As shown in Ref. [13], Eq. (C3) can be written as

$$\mathbb{E}_U(F_g) = \mathbf{Tr}[\rho \hat{\Lambda}_{\mathbf{c}}^{\mathbf{avg}} \rho] = F_g(\hat{\Lambda}_{\mathbf{c}}^{\mathbf{avg}}),$$

where $\hat{\Lambda}_{\mathbf{c}}^{\mathbf{avg}} \equiv \int dU \hat{U} \hat{\Lambda}_{\mathbf{c}} \hat{U}^{-1}$. Based on the analysis of $\hat{\Lambda}_{\mathbf{c}}^{\mathbf{avg}}$ in Ref. [13], the noisy channel $\hat{\Lambda}_{\mathbf{c}}^{\mathbf{avg}}$ can be written as follows

$$\hat{\Lambda}_{\mathbf{c}}^{\mathbf{avg}} \rho = p\rho + (1-p)\frac{\mathbb{I}}{D}, \tag{C4}$$

where p can be seen as the strength of the depolarizing channel. By applying the channel n times, we can obtain the fidelity in the form

$$F_n = p^n \mathbf{Tr}[\rho(0)^2] + \frac{(1-p^n)}{D}.$$

If $p = 1$ then the fidelity F_n is equal to 1, which means there is no error. It is worth noting that the mathematical form of the depolarizing channel in Ref. [13] is different from the mathematical form in Ref. [30], where it is written as

$$\Lambda_{\mathbf{c},p}^{d}(\rho) = (1-p)\rho + p\mathbf{Tr}(\rho)\frac{I_d}{d}, \tag{C5}$$

where d is the dimension of the Hilbert space and p is the depolarizing probability. Therefore, the physical interpretations of these two mathematical forms may be a little different. So far we have mentioned the relation between the average gate fidelity and the depolarizing channel; and the physical meaning p in the depolarizing channel written as Eqs. (C4) and (C5), respectively. Now we can use the equivalence mentioned in Ref. [13]

$$\mathbb{E}_{\psi}(F_g) = \mathbb{E}_U(F_g), \tag{C6}$$

where

$$\mathbb{E}_{\psi}(F_g) \equiv \int d\psi \langle\psi|U^{-1}(\Lambda(U|\psi\rangle\langle\psi|U^{-1}))U|\psi\rangle. \tag{C7}$$

The measure $d\psi$ in Eq. (C7) is unitarily invariant over the set of pure states, and $|\psi\rangle$ is a quantum state.

Finally, we can fit our results of the zero-fidelity to exponential decay curve $Ap^n + B$, where p is the strength of depolarization and n is the number of repeated applications of circuits (identity folding), and A, B are caused by SPAM errors as long as our noisy channel is the depolarizing channel [8]. So, for the ideal situation (without depolarizing noise and SPAM errors), the fidelity is $p = 1$. Furthermore, based on the analysis in Ref. [13], we can explain the relation between quantum state 2-design (recall that SIC-state are quantum state 2-design) and unitary 2-design. So we can twirl the noise channel into depolarizing channel [13]. We can conclude that zero noise extrapolation can be used to obtain the channel fidelity from the decay rate of the zero-fidelity without considering the effects from SPAM errors.

[1] S. T. Flammia and Y.-K. Liu, Direct fidelity estimation from few pauli measurements, Phys. Rev. Lett. **106**, 230501 (2011).

[2] S. Greenaway, F. Sauvage, K. E. Khosla, and F. Mintert, Efficient assessment of process fidelity, Phys. Rev. Res. **3**, 033031 (2021).

[3] E. Nielsen, J. K. Gamble, K. Rudinger, T. Scholten, K. Young, and R. Blume-Kohout, Gate Set Tomography, Quantum **5**, 557 (2021).

[4] J. M. Renes, R. Blume-Kohout, A. J. Scott, and C. M. Caves, Symmetric informationally complete quantum measurements, Journal of Mathematical Physics **45**, 2171 (2004), https://pubs.aip.org/aip/jmp/article-pdf/45/6/2171/8173125/2171_1_online.pdf.

[5] E. Knill, D. Leibfried, R. Reichle, J. Britton, R. B. Blakestad, J. D. Jost, C. Langer, R. Ozeri, S. Seidelin, and D. J. Wineland, Randomized benchmarking of quantum gates, Phys. Rev. A **77**, 012307 (2008).

[6] E. Kawakami, T. Jullien, P. Scarlino, D. R. Ward, D. E. Savage, M. G. Lagally, V. V. Dobrovitski, M. Friesen, S. N. Coppersmith, M. A. Eriksson, and L. M. K. Vandersypen, Gate fidelity and coherence of an electron spin in an si/sige quantum dot with micromagnet, Proceedings of the National Academy of Sciences **113**, 11738 (2016), https://www.pnas.org/doi/pdf/10.1073/pnas.1603251113.

[7] T. F. Watson, S. G. J. Philips, E. Kawakami, D. R. Ward, P. Scarlino, M. Veldhorst, D. E. Savage, M. G. Lagally, M. Friesen, S. N. Coppersmith, M. A. Eriksson, and L. M. K. Vandersypen, A programmable two-qubit quantum processor in silicon, Nature **555**, 633 (2018).

[8] T. Giurgica-Tiron, Y. Hindy, R. LaRose, A. Mari, and W. J. Zeng, Digital zero noise extrapolation for quantum error mitigation, 2020 IEEE International Conference on Quantum Computing and Engineering (QCE) , 306 (2020).

[9] A. Erhard, J. J. Wallman, L. Postler, M. Meth, R. Stricker, E. A. Martinez, P. Schindler, T. Monz, J. Emerson, and R. Blatt, Characterizing large-scale quantum computers via cycle benchmarking, Nature Communications **10**, https://doi.org/10.1038/s41467-019-13068-7 (2019).

[10] O. Di Matteo, A short introduction to unitary 2-designs, unpublished, https://api.semanticscholar.org/CorpusID:52059910, (accessed: June 2024) (2014).

[11] A. Klappenecker and M. Rotteler, Mutually unbiased bases are complex projective 2-designs, in *Proceedings. International Symposium on Information Theory, 2005. ISIT 2005.* (2005) pp. 1740–1744.

[12] All simulations in this paper were performed using IBM Qiskit.

[13] J. Emerson, R. Alicki, and K. Życzkowski, Scalable noise estimation with random unitary operators, Journal of Optics B: Quantum and Semiclassical Optics **7**, S347 (2005).

[14] M. D. Bowdrey, D. K. Oi, A. Short, K. Banaszek, and J. Jones, Fidelity of single qubit maps, Physics Letters A **294**, 258 (2002).

[15] E. Magesan, J. M. Gambetta, and J. Emerson, Characterizing quantum gates via randomized benchmarking, Phys. Rev. A **85**, 042311 (2012).

[16] S. Aaronson and D. Gottesman, Improved simulation of stabilizer circuits, Phys. Rev. A **70**, 052328 (2004).

[17] Qiskit contributors, Qiskit: An open-source framework for quantum computing (2023).

[18] A. Javadi-Abhari, M. Treinish, K. Krsulich, C. J. Wood, J. Lishman, J. Gacon, S. Martiel, P. D. Nation, L. S. Bishop, A. W. Cross, B. R. Johnson, and J. M. Gambetta, Quantum computing with Qiskit (2024), arXiv:2405.08810 [quant-ph].

[19] D. C. McKay, S. Sheldon, J. A. Smolin, J. M. Chow, and J. M. Gambetta, Three-qubit randomized benchmarking, Phys. Rev. Lett. **122**, 200502 (2019).

[20] S. Endo, S. C. Benjamin, and Y. Li, Practical quantum error mitigation for near-future applications, Phys. Rev. X **8**, 031027 (2018).

[21] K. Temme, S. Bravyi, and J. M. Gambetta, Error mitigation for short-depth quantum circuits, Phys. Rev. Lett. **119**, 180509 (2017).

[22] Z. Li, P. Liu, P. Zhao, Z. Mi, H. Xu, X. Liang, T. Su, W. Sun, G. Xue, J. Zhang, W. Liu, Y. Jin, and H. Yu, Error per single-qubit gate below $10^{-}4$ in a superconducting qubit, npj Quantum Information **9**, 1 (2023).

[23] A. Bourassa, C. P. Anderson, K. C. Miao, M. Onizhuk, H. Ma, A. L. Crook, H. Abe, J. UlHassan, T. Ohshima, N. T. Son, G. Galli, and D. D. Awschalom, Entanglement and control of single nuclear spins in isotopically engineered silicon carbide, Nature materials **19**, 1319—1325 (2020).

[24] E. Magesan, J. M. Gambetta, B. R. Johnson, C. A. Ryan, J. M. Chow, S. T. Merkel, M. P. da Silva, G. A. Keefe, M. B. Rothwell, T. A. Ohki, M. B. Ketchen, and M. Steffen, Efficient measurement of quantum gate error by interleaved randomized benchmarking, Phys. Rev. Lett. **109**, 080505 (2012).

[25] R. Barends, J. Kelly, A. Megrant, A. Veitia, D. Sank, E. Jeffrey, T. White, J. Mutus, A. Fowler, B. Campbell, Y. Chen, Z. Chen, B. Chiaro, A. Dunsworth, C. Neill, P. O'Malley, P. Roushan, A. Vainsencher, J. Wenner, A. Korotkov, A. Cleland, and J. M. Martinis, Superconducting quantum circuits at the surface code threshold for fault tolerance, Nature **508**, 500—503 (2014).

[26] E. Bannai and E. Bannai, A survey on spherical designs and algebraic combinatorics on spheres, Eur. J. Comb. **30**, 1392 (2009).

[27] A. Roy and S. Suda, Complex spherical designs and codes, J Comb Des **22**, 105 (2013).

[28] A. A. Mele, Introduction to haar measure tools in quantum information: A beginner's tutorial, Quantum **8**, 1340 (2024).

[29] J. Haferkamp, Random quantum circuits are approximate unitary t-designs in depth $O\left(nt^{5+o(1)}\right)$, Quantum **6**, 795 (2022).

[30] J. Etxezarreta Martinez, A. deMarti iOlius, and P. M. Crespo, Superadditivity effects of quantum capacity decrease with the dimension for qudit depolarizing channels, Phys. Rev. A **108**, 032602 (2023).